

# $^{64}\text{Ni}+^{64}\text{Ni}$ fusion reaction calculated with the density-constrained time-dependent Hartree-Fock formalism

A.S. Umar and V.E. Oberacker

*Department of Physics and Astronomy, Vanderbilt University, Nashville, Tennessee 37235, USA*

(Dated: October 30, 2018)

We study fusion reactions of the  $^{64}\text{Ni}+^{64}\text{Ni}$  system using the density-constrained time-dependent Hartree-Fock (TDHF) formalism. In this formalism the fusion barriers are directly obtained from TDHF dynamics. In addition, we incorporate the entrance channel alignments of the slightly deformed (oblate)  $^{64}\text{Ni}$  nuclei due to dynamical Coulomb excitation. We show that alignment leads to a fusion barrier distribution and alters the naive picture for defining which energies are actually sub-barrier. We also show that core polarization effects could play a significant role in fusion cross section calculations.

PACS numbers: 21.60.-n, 21.60.Jz

## I. INTRODUCTION

Radioactive ion-beam facilities enable us to study the structure and reactions of exotic nuclei, in particular the physics properties of the “terra incognita” of neutron-rich isotopes [1]. One important aspect of these studies is a detailed investigation of the heavy-ion fusion process of exotic nuclei. This is crucial not only for superheavy element formation, but it will also lead to a better understanding of the effective  $N - N$  interactions in neutron-rich nuclei and of enhanced correlations present in these many-body systems.

Recently, fusion evaporation cross sections for the  $^{64}\text{Ni}+^{64}\text{Ni}$  system have been measured down to the 10 nb level [2]. This experiment confirmed and improved the earlier data [3] for the same system and it extended the data to extreme sub-barrier energies, thus providing a challenge for the theoretical understanding of the fusion process between two open-shell nuclei. The primary observation was a *hindrance* of fusion in the  $^{64}\text{Ni}+^{64}\text{Ni}$  system at extreme sub-barrier energies in comparison to reactions involving other Nickel isotopes such as the  $^{58}\text{Ni}+^{58}\text{Ni}$  system. Earlier coupled-channels calculations [4, 5] failed to reproduce the data at the extreme sub-barrier energies.

Various hypotheses were developed for the explanation of the fusion hindrance phenomenon. In Ref. [6] the hindrance was attributed to the differing stiffness of Nickel isotopes due to nuclear structure effects. An excellent coupled-channels fit to the data was obtained by supplementing the effective  $N - N$  force used in the double-folding potential with a repulsive core to account for the nuclear incompressibility effects at the nuclear overlap, thus leading to a shallow potential pocket. On the other hand, Refs. [7, 8] suggest that at such low energies the inner turning point of the heavy-ion potential is smaller than the touching point  $r_t = R_1 + R_2$ . Thus the validity of the frozen-density approximation used in Ref. [6] becomes questionable. These authors have proposed a two-step model for fusion in which the effects of neck formation are approximately included [7].

The theoretical analysis of the fusion data generally in-

volves the determination of a phenomenological ion-ion potential such as the Bass model [9, 10], the proximity potential [11, 12, 13, 14], or potentials obtained via the double-folding method [15, 16, 17, 18]. Subsequently, the actual fusion cross section is calculated by either using barrier penetration models [10, 17, 19, 20], or the coupled-channel method [4, 5, 21, 22, 23]. The latter includes various excitations of the target and/or projectile using the coupled-channel formalism [4, 23], as well as the inclusion of neutron transfer, and can be consistently applied at energies above and below the barrier [20]. Effectively, the inclusion of each additional excitation leads to a modification of the original inert core ion-ion potential, resulting in a series of effective barriers. One common physical assumption used in many of these calculations is the use of the frozen density or the sudden approximation. In this approximation the nuclear densities are unchanged during the computation of the ion-ion potential as a function of the internuclear distance. Furthermore, the effects included in channel couplings are usually based on the static properties of the participating nuclei, which may accurately represent the early stages of the collision process, but are expected to change as the two ions strongly interact. While these methods provide a useful and productive means for quantifying multitudinous reaction data it is desirable to include dynamical effects and make contact with the microscopic theories of nuclear structure and reactions.

Recently, we have developed a microscopic approach for calculating heavy-ion interaction potentials which incorporates all of the dynamical entrance channel effects included in the time-dependent Hartree-Fock (TDHF) description of the collision process [24]. These effects include the neck formation, particle exchange, internal excitations, and deformation effects to all order, as well as the effect of nuclear alignment for deformed systems. The method is based on the TDHF evolution of the nuclear system coupled with density-constrained Hartree-Fock calculations to obtain the ion-ion interaction potential. Preliminary calculations for the  $^{64}\text{Ni}+^{132}\text{Sn}$  system highlighted the importance of dynamical deformation effects [25, 26]. Here we give a completed study of fusion

cross sections using this formalism.

In the next section we will summarize some theoretical aspects of the density-constrained TDHF theory along with methods to incorporate dynamical alignment into our calculations, as well as the method used to calculate cross sections from the resulting barriers. In Section III we present interesting aspects of the reaction dynamics and compare our results with experiment and other calculations. In section IV we summarize our conclusions.

## II. THEORETICAL METHODS

### A. Density-constrained TDHF method

For the calculations of dynamical potential barriers for the  $^{64}\text{Ni}+^{64}\text{Ni}$  system we have used the density-constrained TDHF (DC-TDHF) method. Further details of the method can be found in Ref. [24], here we give a short overview.

The *density constraint* is a novel numerical method that was developed in the mid 1980's [27, 28] and was used to provide a microscopic description of the formation of shape resonances in light systems [28]. In this approach the TDHF time-evolution takes place with no restrictions. At certain times during the evolution the instantaneous density is used to perform a static Hartree-Fock minimization while holding the total density constrained to be the instantaneous TDHF density. In essence, this provides us with the TDHF dynamical path in relation to the multi-dimensional static energy surface of the combined nuclear system. Since we are constraining the total density all moments are simultaneously constrained. The numerical procedure for implementing this constraint and the method for steering the solution to  $\rho_{\text{TDHF}}(\mathbf{r}, t)$  is discussed in Refs. [27, 28]. The convergence property is as good if not better than in the traditional constrained Hartree-Fock calculations with a constraint on a single collective degree of freedom.

In Ref. [24] we have shown that the ion-ion interaction potential is given by

$$V(R) = E_{\text{DC}}(R) - E_{A_1} - E_{A_2}, \quad (1)$$

where  $E_{\text{DC}}$  is the density-constrained energy at the instantaneous separation  $R(t)$ , while  $E_{A_1}$  and  $E_{A_2}$  are the binding energies of the two nuclei obtained with the same effective interaction. We would like to emphasize again that this procedure does not affect the TDHF time-evolution and contains no *free parameters* or *normalization*. In practice, TDHF runs are initialized with energies above the Coulomb barrier and in Ref. [24] we have shown that there is no appreciable energy dependence to the barriers obtained via the density-constrained TDHF method. The separation coordinate  $R$  is the distance between the centers of mass of the two nuclei.

### B. Fusion for deformed nuclei

The heavy-ion interaction potential between two deformed nuclei depends on the distance vector between their centers-of-mass,  $\mathbf{R}$ , and on the relative orientation of their intrinsic principal axis systems which may be described in terms of three Euler angles  $(\alpha, \beta, \gamma)$  per nucleus, i.e. in the most general case we have

$$V = V(\mathbf{R}, \alpha_1, \beta_1, \gamma_1, \alpha_2, \beta_2, \gamma_2). \quad (2)$$

The expression for  $V$  can be simplified if the intrinsic nuclear density distributions are axially symmetric; in this case, the potential does not depend on the Euler angles  $\gamma_1, \gamma_2$  which describe rotations about the symmetry axes. If we put, for convenience, the distance vector in  $z$ -direction,  $\mathbf{R} = R\mathbf{e}_z$ , the potential between two deformed axially symmetric nuclei has the structure

$$V = V(R, \beta_1, \beta_2, \Delta\alpha). \quad (3)$$

The heavy-ion interaction potential is calculated with the density-constrained TDHF method for a given set of orientation angles  $\beta_1, \beta_2, \Delta\alpha$ . Fortunately, test calculations using the double-folding method described in Ref. [18] reveal that the dependence on the Euler angle  $\Delta\alpha$  is negligible in our case so we put  $\Delta\alpha = 0$ . In Fig. 1 we show the definition of the angles  $\beta_1$  and  $\beta_2$  for two oblate nuclei.

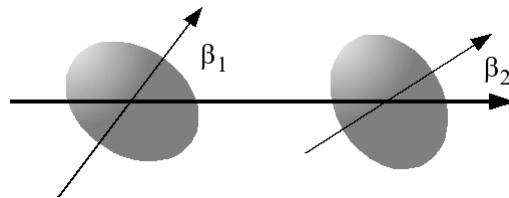


FIG. 1: Shown are the orientation angles  $\beta_1$  and  $\beta_2$  of the oblate Ni nuclei with respect to the collision axis.

In order to calculate the total fusion cross section at energy  $E_{\text{c.m.}}$ , we first consider the partial cross section for given initial orientations  $(\beta_1, \beta_2)$  of the two nuclei which is given by

$$\sigma(E_{\text{c.m.}}, \beta_1, \beta_2) = \frac{\pi}{k_0^2} \sum_{L=0}^{\infty} (2L+1) T_L(E_{\text{c.m.}}, \beta_1, \beta_2), \quad (4)$$

with  $k_0 = \sqrt{2\mu E_{\text{c.m.}}}$ . The fusion barrier penetrabilities  $T_L(E_{\text{c.m.}}, \beta_1, \beta_2)$  are obtained by numerical integration of the two-body Schrödinger equation using the *incoming wave boundary condition* (IWBC) method [21, 29]

$$\left[ \frac{-\hbar^2}{2\mu} \frac{d^2}{dR^2} + \frac{L(L+1)\hbar^2}{2\mu R^2} + V(R, \beta_1, \beta_2) - E \right] \psi = 0,$$

where the quantity  $V(R, \beta_1, \beta_2)$  denotes the heavy-ion potential obtained via the density-constrained TDHF method. For the numerical implementation we have followed the procedure for the coupled-channel code CC-FUL described in Ref. [23]. IWBC assumes that once the

minimum of the potential is reached fusion will occur. In practice, the Schrödinger equation is integrated from the potential minimum,  $R_{\min}$ , where only an incoming wave is assumed, to a large asymptotic distance, where it is matched to incoming and outgoing Coulomb wavefunctions. The barrier penetration factor,  $T_L(E_{c.m.}, \beta_1, \beta_2)$  is the ratio of the incoming flux at  $R_{\min}$  to the incoming Coulomb flux at large distance.

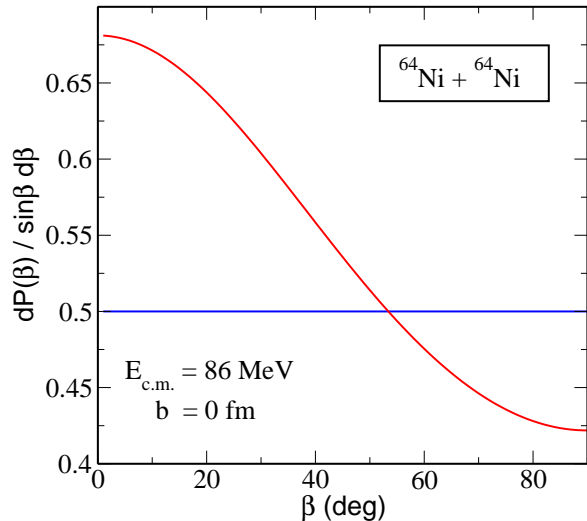


FIG. 2: (Color online) Dynamic alignment due to Coulomb excitation of  $^{64}\text{Ni}$ . Shown is the orientation probability as a function of the Euler angle  $\beta$  in a central collision at internuclear distances  $R = 1500$  fm (blue curve) and at  $R = 16$  fm (red curve).

Once the partial fusion cross sections (4) for given orientation angles  $(\beta_1, \beta_2)$  have been calculated, we have to take an average over all initial angular orientations of both nuclei

$$\sigma(E_{c.m.}) = \int_0^\pi \sin(\beta_1) d\beta_1 \int_0^\pi \sin(\beta_2) d\beta_2 \times \frac{d^2 P(E_{c.m.}, \beta_1, \beta_2)}{\sin(\beta_1) d\beta_1 \sin(\beta_2) d\beta_2} \sigma(E_{c.m.}, \beta_1, \beta_2),$$

where  $d^2 P(E_{c.m.}, \beta_1, \beta_2)$  represents the alignment probability for both deformed nuclei. Details of the dynamic alignment formalism are presented in [30]. We give here a brief summary: For a given incident energy  $E_{c.m.}$  we carry out a semiclassical Coulomb excitation calculation of the dominant collective levels of the deformed nucleus. The energy levels and  $EL$ -transition matrix elements for  $^{64}\text{Ni}$  are taken from experimental data [31]:  $E_{2+} = 1.346$  MeV,  $E_{4+} = 2.610$  MeV and  $M(E2, 0+ \rightarrow 2+) = -27.0 e fm^2$  (oblate deformation). The Coulomb excitation calculation starts at very large internuclear distances (about 1500 fm) when both nuclei may be presumed to be in their respective ground states and stops at the ion-ion separation distance  $R(t_0)$  (about 16 fm). The Coulomb excitation amplitudes determine the probability distribution of initial orientations. Using

the dominant monopole-multipole part of the Coulomb interaction, the orientation probability factorizes as follows

$$\frac{d^2 P(E_{c.m.}, \beta_1, \beta_2)}{\sin(\beta_1) d\beta_1 \sin(\beta_2) d\beta_2} = \frac{dP_1(E_{c.m.}, \beta_1)}{\sin(\beta_1) d\beta_1} \frac{dP_2(E_{c.m.}, \beta_2)}{\sin(\beta_2) d\beta_2}.$$

In the special case of no preferential alignment, i.e. all initial orientation angles are equally likely, this factor reduces to

$$\left. \frac{d^2 P(E_{c.m.}, \beta_1, \beta_2)}{\sin(\beta_1) d\beta_1 \sin(\beta_2) d\beta_2} \right|_{\text{noalign}} \rightarrow \frac{1}{4}.$$

In Fig. 2 we show the differential alignment probability as a function of the Euler angle  $\beta$  used in our calculations.

### III. RESULTS

We have carried out a number of TDHF calculations with accompanying density constraint calculations to compute  $V(R, \beta_1, \beta_2)$  given by Eq. (1). A detailed description of our new three-dimensional unrestricted TDHF code has recently been published in Ref [32]. The code was modified to self-consistently generate initial states for  $^{64}\text{Ni}$  with different orientations. For the effective interaction we have primarily used the Skyrme SLy5 force [33], including all of the time-odd terms. In this case the  $^{64}\text{Ni}$  nucleus is essentially oblate having a quadrupole moment of  $-0.45$  b. This is also confirmed by other calculations [34, 35].

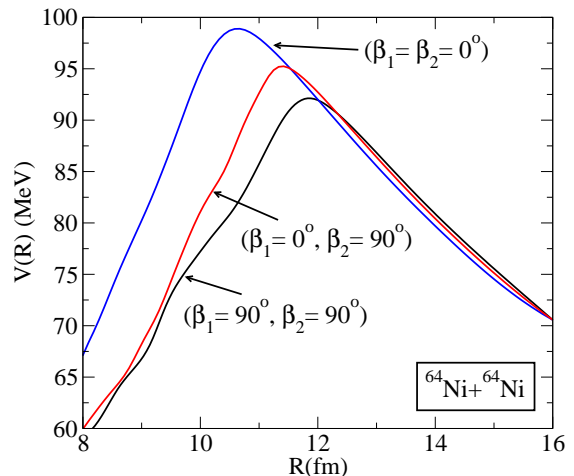


FIG. 3: (Color online) Potential barriers,  $V(R, \beta_1, \beta_2)$ , obtained from density-constrained TDHF calculations for the  $^{64}\text{Ni} + ^{64}\text{Ni}$  system. The Euler angles  $\beta_1$  and  $\beta_2$  indicate different orientations of the deformed  $^{64}\text{Ni}$  nucleus.

All of our TDHF calculations were done at an initial energy of  $E_{c.m.} = 98$  MeV and separation  $R(t_0) = 16$  fm. As we have reported in Ref. [24] the potential barriers obtained from the density-constrained TDHF method are not sensitive to the initial energy (above the barrier).

We have tested this again by running a few orientations at 112 MeV and did not observe any appreciable difference. In Fig. 3 we show the barriers obtained for limiting orientations of the  $^{64}\text{Ni}$  nuclei. We have also calculated these limiting barriers using other effective interactions, SkM\* [36] and SLy4 [33], with essentially no difference. While most modern Skyrme parametrizations give essentially the same potential barrier, using an older Skyrme force such as the SIII [37] interaction results in a higher barrier and consequently lower fusion cross sections. This issue will be discussed later in the manuscript.

The physical picture which emerges from the barriers shown in Fig. 3 is that the total fusion cross section strongly depends on the deformation phase space. It also shows the fallacy of the often-used statement that a certain energy is *sub-barrier*, which stems from spherical systems that can be studied using a single barrier. For deformed systems this is dependent on the orientation of the nuclei. For the  $^{64}\text{Ni}+^{64}\text{Ni}$  system the only truly sub-barrier energies are those below the lowest potential barrier corresponding to the  $\beta_1 = \beta_2 = 90^\circ$  orientation, about  $E_{c.m.} = 92$  MeV. The fusion cross sections corresponding to energies above the lowest barrier will be dominated by it since above-barrier cross sections are much larger than the below-barrier ones.

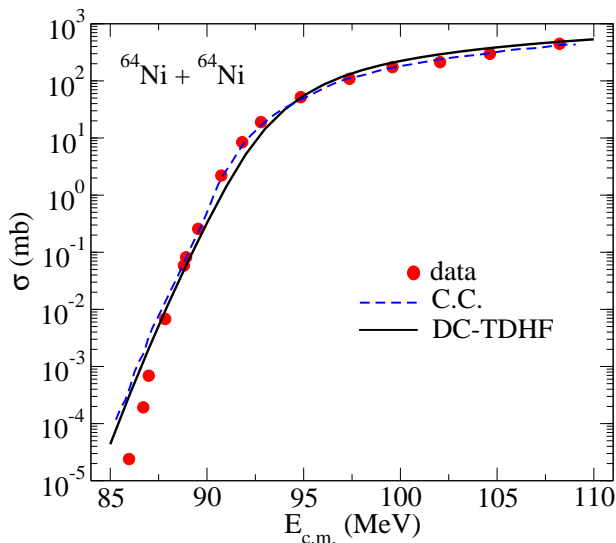


FIG. 4: (Color online) Total fusion cross section as a function of  $E_{c.m.}$ . Shown are the experimental data (filled red circles) and the coupled-channel calculation from Ref. [2] (blue dashed curve), and fusion cross sections calculated with the density-constrained TDHF method using the SLy5 force (solid black line).

For the calculation of barrier distributions as a function of the orientations angles  $\beta_1$  and  $\beta_2$  we have chosen an angular spacing of  $\Delta\beta = 10^\circ$ . In principle this requires four hundred DC-TDHF calculations, which would be very time consuming. However, one can show that some of the orientations are equivalent to each other. One major assumption we have made is to assume the equality of

the angular intervals  $(0, \pi/2)$  and  $(\pi/2, \pi)$ , which is not exactly correct when both nuclei are deformed. In order to assure that this approximation does not effect the lowest energy cross sections (primarily determined by the lowest barrier) we have explicitly calculated those angles that would have appreciable contribution at these energies. In total we have computed twenty potential barriers corresponding to various orientations for the SLy5 force. In principle even this may not be necessary since all of the barriers must fall between the limiting cases shown in Fig. 3. Although actual calculations show that a constant angular interval  $\Delta\beta$  does not always lead to equally spaced barriers such an extrapolation has a minimal effect on the actual cross section calculations. We have confirmed this by generating such barriers from the limiting barriers using a numerical averaging procedure and calculating the fusion cross section. This method was used for the calculation of the cross sections for the SIII interaction.

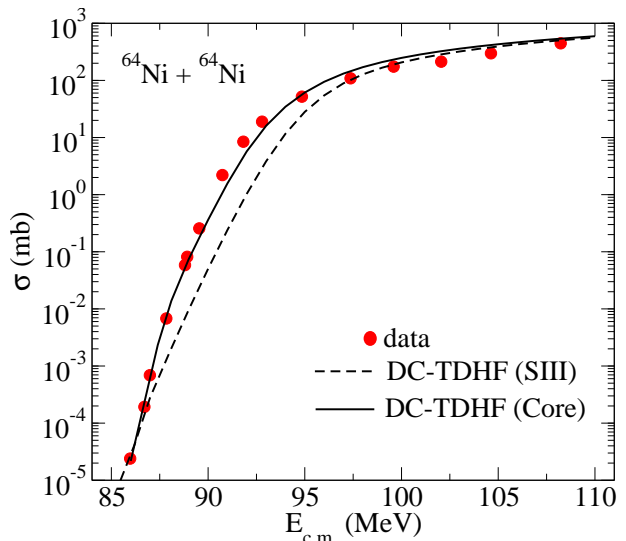


FIG. 5: (Color online) Total fusion cross section as a function of  $E_{c.m.}$ . Shown are the experimental data (filled red circles), density-constrained TDHF cross sections using the SIII force (dashed black line), and the density-constrained TDHF cross sections using the core orientation with the SLy5 force for the lowest energy cross sections.

In Fig. 4 we show the total DC-TDHF fusion cross section as a function of the center-of-mass energy (solid black curve) using the SLy5 force. Also, shown are the experimental data (filled circles), and the coupled-channels calculations of Ref. [2] (dashed blue line). Results for SLy4 and SkM\* interactions are indistinguishable from the SLy5 result. We observe that the DC-TDHF calculations, which contain no parameters or normalization, accurately reproduce the fusion cross sections for all energies except for energies  $E_{c.m.} \leq 87$  MeV. We believe that the small deviations at other energies are largely due to the symmetry assumptions made in alignment averaging. As we stated earlier this is not the case

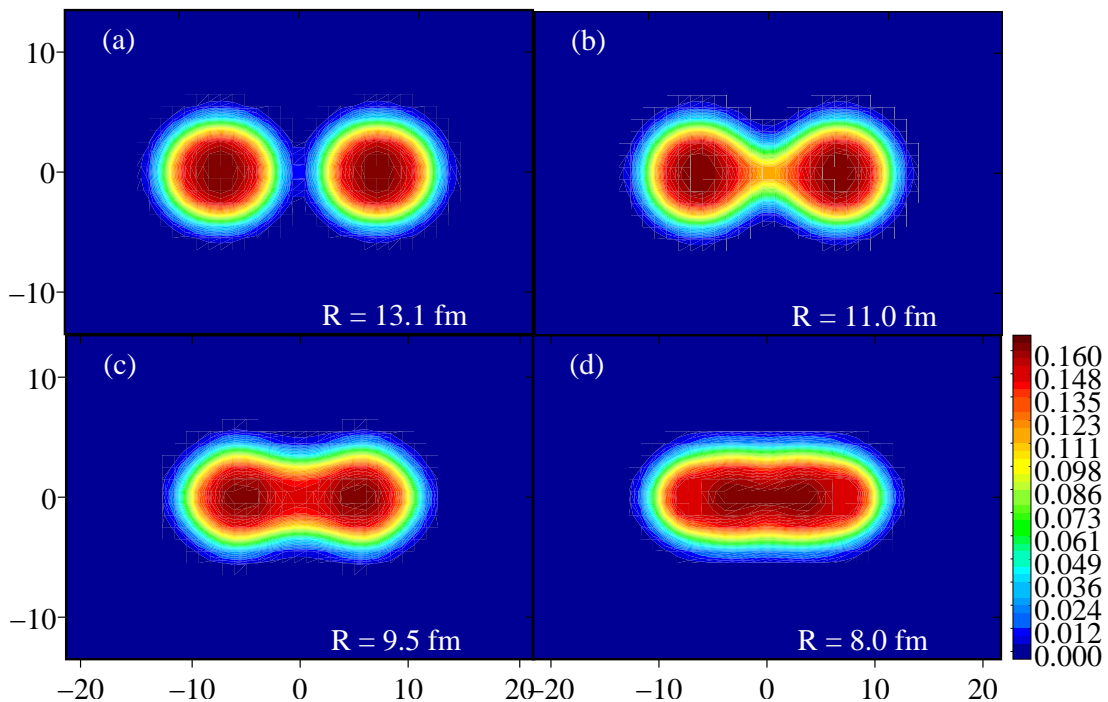


FIG. 6: (Color online) Shown are the density contours in the  $x - z$  plane for the TDHF time-evolution of the  $^{64}\text{Ni}+^{64}\text{Ni}$  system. Initially both nuclei are oriented with angles  $\beta_1 = \beta_2 = 90^\circ$  at a center-of-mass energy of  $E_{c.m.} = 98$  MeV. The values for the ion-ion separation  $R$  correspond to special points along the potential barrier at the lowest experimental energy of  $E_{c.m.} = 86$  MeV; (a) outer turning point, (b) inner turning point, (c) reorientation of the core, and (d) potential minimum.

for the lowest energies as these were explicitly done without symmetry assumptions.

In Ref. [6] the hindrance of the fusion cross section at deep sub-barrier energies was attributed to nuclear incompressibility effects at the nuclear overlap and in Ref. [8] to the modifications of the inner turning point in comparison to standard folding model calculations using the frozen-density approximation. As we shall see below, both of these assertions may be correct. In order to investigate the dependence on incompressibility we have repeated our calculations using an older Skyrme parametrization, SIII [37], having a nuclear matter incompressibility coefficient of 356 MeV, as opposed to most of the modern Skyrme parametrizations that have nuclear matter incompressibility around 230 MeV. Although the SIII interaction accurately reproduces many spectroscopic properties of spherical and close to spherical nuclei it is known not to correctly reproduce fission barriers and other phenomena involving large deformations. In Fig. 5 the black dashed line corresponds to the DC-TDHF calculations using the SIII interaction. As we see, this interaction underestimates the fusion cross sections at intermediate energies but does relatively well at low and high energies. Although it is difficult to disentangle the effect of incompressibility from all the other aspects of the effective interaction, one may conclude that a new Skyrme force with a higher than the accepted nuclear matter incompressibility of 230 MeV and fitted to repro-

duce large amplitude collective phenomena could better reproduce the fusion cross sections.

In order to better examine the evolution of the nuclear density, in Fig. 6 we have plotted the nuclear density at four special internuclear distances  $R$  for the  $\beta_1 = \beta_2 = 90^\circ$  initial orientation. Frame (a) corresponds to the nuclear density at the outer turning point of the ion-ion potential ( $R = 13.1$  fm) at  $E_{c.m.} \leq 86$  MeV. One striking observation from this frame is that the orientation of the nuclear core seems to be rotated in comparison to the total nuclear density by  $\pi/2$ . Frame (b) of Fig. 6 shows the total density at the ion-ion separation of  $R = 11.0$  fm, which approximately corresponds to the location of the inner turning point at  $E_{c.m.} \leq 86$  MeV. The orientation of the nuclear core is still the same as at the outer turning point. At around  $R = 10$  fm the nuclear core rotates and aligns with the total nuclear density. In frame (c) we show this at  $R = 9.5$  fm. The last frame (d) shows the nuclear density at the potential minimum which occurs around  $R = 8.0$  fm. Based on the above observation we can make a conjecture that while at higher energies the potential barrier is largely determined by the nuclear surface at deep barrier energies core nucleons play a significant role in barrier dynamics. This may manifest itself as repulsive core in constructing a potential model for the problem. In our calculations we can incorporate this effect by using the alignment angles of the core rather than the total density in the calculation

of the cross sections at the lowest energies. This is shown by the black solid curve in Fig. 5. As we see the results are in excellent agreement with the data at low energies.

#### IV. CONCLUSIONS

As we investigate fusion reactions involving neutron rich and deformed nuclei it is apparent that an understanding of the structure of these nuclei is crucial to the description of the reaction dynamics. For these nuclei various effects, such as inelastic excitations, particle transfer, and other dynamical effects lead to substantial modification of the naive potential barrier calculations which assume an inert core and no dynamics. Consequently, the definition of *sub-barrier* fusion becomes ambiguous since it is difficult to determine the barrier a priori.

We have performed density-constrained TDHF calculations of fusion cross sections for the  $^{64}\text{Ni}+^{64}\text{Ni}$  system. Our results agree well with the measured data despite having no adjustable parameters. This indicates that many of the reaction dynamics are included in the TDHF evolution of the nuclear density. We have also investigated the dependence of our results on the microscopic effective interaction. We find that while all of the modern Skyrme parametrizations show very small deviations in the fusion cross sections, which was also observed in a more systematic study of spherical systems [32], the older parametrizations yield very different results. Since older

Skyrme parametrizations were fitted mostly to reproduce properties of spherical nuclei they may not be a good candidate for fusion studies. On the other hand it may be desirable to investigate the dependence on incompressibility using a more modern Skyrme parametrization, which is not yet available.

We have further investigated fusion cross sections at deep sub-barrier energies. In the absence of a true many-body tunneling approach to nuclear fusion it is difficult to envision the dynamical formation of the potential barrier at very deep sub-barrier energies. As we go further down in energy the inner turning point of the ion-ion potential involves larger overlaps between the participating nuclei. Consequently, core nucleons may play a more dominant role in dynamically building up the potential barrier. In the case of  $\beta_1 = \beta_2 = 90^\circ$  corresponding to the lowest potential barrier we observed that the nuclear core has a different orientation from the total nuclear density. Based on this observation we have speculated that at the lowest energies it may make sense to use the orientation of the core rather than the nuclear surface. This core polarization effect allows us to reproduce the experimental cross sections at the lowest energies.

#### Acknowledgments

This work has been supported by the U.S. Department of Energy under grant No. DE-FG02-96ER40963 with Vanderbilt University.

- 
- [1] *Opportunities in Nuclear Science, A Long-Range Plan for the Next Decade*, DOE/NSF Nuclear Science Advisory Committee, April 2002, [www.sc.doe.gov/production/henp/np/nsac/nsac.html](http://www.sc.doe.gov/production/henp/np/nsac/nsac.html).
- [2] C. L. Jiang *et al.*, Phys. Rev. Lett. **93**, 012701 (2004).
- [3] M. Beckerman, M. Salomaa, A. Sperduto, J. D. Molitoris, and A. DiRienzo, Phys. Rev. C **25**, 837 (1982).
- [4] H. Esbensen, Prog. Theor. Phys. Suppl. **154**, 11 (2004).
- [5] H. Esbensen, Phys. Rev. C **72**, 054607 (2005).
- [6] Ş. Mişicu and H. Esbensen, Phys. Rev. Lett. **96**, 112701 (2006).
- [7] Takatoshi Ichikawa, Kouichi Hagino, and Akira Iwamoto, Phys. Rev. C **75**, 057603 (2007).
- [8] Takatoshi Ichikawa, Kouichi Hagino, and Akira Iwamoto, Phys. Rev. C **75**, 064612 (2007).
- [9] R. Bass, Nucl. Phys. **A231**, 45 (1974).
- [10] R. Bass, *Nuclear Reactions with Heavy Ions*, (Springer Verlag, New York, 1980).
- [11] J. Blocki, J. Randrup, W. J. Swiatecki, and C. F. Tsang, Ann. Phys. (N.Y.) **105**, 427 (1977).
- [12] J. Randrup and J. S. Vaagen, Phys. Lett. **B77**, 170 (1978).
- [13] M. Seiwert, W. Greiner, V. E. Oberacker, and M. J. Rhoades-Brown, Phys. Rev. C **29**, 477 (1984).
- [14] J. R. Birkelund and J. R. Huizenga, Phys. Rev. C **17**, 126 (1978).
- [15] G. R. Satchler and W. G. Love, Phys. Rep. **55**, 183 (1979).
- [16] G. Bertsch, J. Borysowicz, H. McManus, and W. G. Love, Nucl. Phys. **A284**, 399 (1977).
- [17] M. J. Rhoades-Brown and V. E. Oberacker, Phys. Rev. Lett. **50**, 1435 (1983).
- [18] M. J. Rhoades-Brown, V. E. Oberacker, M. Seiwert, and W. Greiner, Z. Phys. A **310**, 287 (1983).
- [19] N. Takigawa and G. F. Bertsch, Phys. Rev. C **29**, 2358 (1984).
- [20] A. B. Balantekin and N. Takigawa, Rev. Mod. Phys. **70**, 77 (1998).
- [21] S. Landowne and S. C. Pieper, Phys. Rev. C **29**, 1352 (1984).
- [22] M. J. Rhoades-Brown and M. Prakash, Phys. Rev. Lett. **53**, 333 (1984).
- [23] K. Hagino, N. Rowley, and A. T. Kruppa, Comp. Phys. Comm. **123**, 143 (1999).
- [24] A. S. Umar and V. E. Oberacker, Phys. Rev. C **74**, 021601(R) (2006).
- [25] A. S. Umar and V. E. Oberacker, Phys. Rev. C **74**, 061601(R) (2006).
- [26] A. S. Umar and V. E. Oberacker, Phys. Rev. C **76**, 014614 (2007).
- [27] R. Y. Cusson, P. -G. Reinhard, M. R. Strayer, J. A. Maruhn, and W. Greiner, Z. Phys. A **320**, 475 (1985).
- [28] A. S. Umar, M. R. Strayer, R. Y. Cusson, P. -G. Reinhard, and D. A. Bromley, Phys. Rev. C **32**, 172 (1985).

- [29] G. H. Rawitscher, Phys. Rev. 135, 605 (1964).
- [30] A. S. Umar and V. E. Oberacker, Phys. Rev. C **74**, 024606 (2006).
- [31] Evaluated Nuclear Structure Data File (ENSDF), National Nuclear Data Center, Brookhaven National Laboratory, <http://www.nndc.bnl.gov/ensdf>.
- [32] A. S. Umar and V. E. Oberacker, Phys. Rev. C **73**, 054607 (2006).
- [33] E. Chabanat, P. Bonche, P. Haensel, J. Meyer and R. Schaeffer, Nucl. Phys. **A635**, 231 (1998); Nucl. Phys. **A643**, 441(E) (1998).
- [34] J. Dobaczewski, M. V. Stoitsov, and W. Nazarewicz, *Skyrme-HFB deformed nuclear mass table*, ed. R. Bijker, R.F. Casten, and A. Frank, (AIP, New York, 2004), **726**, 51 (2004).
- [35] G. A. Lalazissis, S. Raman, and P. Ring, At. Data Nucl. Data Tables **71**, 1 (1999).
- [36] J. Bartel, P. Quentin, M. Brack, C. Guet, and H. B. Hakansson, Nucl. Phys. **A386**, 79 (1982).
- [37] M. Beiner, H. Flocard, Nguyen Van Giai, and Ph. Quentin, Nucl. Phys. **A238**, 29 (1975).